

Effective Optical Properties of Non-absorbing Nanoporous Thin-Films

Matthew M. Braun and Laurent Pilon

*Mechanical and Aerospace Engineering Department
420 Westwood Plaza, 37-132 Eng. IV
Henry Samueli School of Engineering and Applied Science
University of California, Los Angeles - Los Angeles, CA 90095, USA
Phone: +1 (310)-206-5598, Fax: +1 (310)-206-2302
E-mail: pilon@seas.ucla.edu*

Abstract

Numerous effective medium models have been proposed for the effective optical properties nanoporous media. However, validations of these models against experimental data are often contradictory and inconclusive. This issue was numerically investigated by solving the two-dimensional Maxwell's equations in non-absorbing nanoporous thin-films with various morphologies. It was found that below a certain critical film thickness, the effective index of refraction depends on the porosity and on the pore size, shape and spatial distribution. For thick enough films the effective index of refraction depends solely on porosity and on the indices of refraction of the two phases. The numerical results agree very well with a recent model obtained by applying the Volume Averaging Theory to the Maxwell's equations. However, commonly used models systematically and sometimes significantly underpredict the numerical results.

Key words: dielectric properties, optical properties, optoelectronic devices

NOMENCLATURE

- a ellipse dimension parallel to incident radiation
- b ellipse dimension perpendicular to incident radiation
- C electrical capacitance
- c speed of light

D	pore diameter
\vec{E}	electric field vector
\vec{H}	magnetic field vector
k	absorption index
L	thickness of a thin-film
m	complex index of refraction
n	real part of the complex index of refraction
\vec{n}	normal vector
r	Fresnel reflection coefficient
R	electrical resistance, reflectance
t	Fresnel transmission coefficient
T	transmittance

Greek symbols

β	phase difference between interfering waves
χ	scattering size parameter
ϵ	electric permittivity
ϕ	porosity
λ	wavelength of the electromagnetic wave
μ	magnetic permeability
$\vec{\pi}$	Poynting vector
ω	angular frequency of electromagnetic wave
ψ	general property

Subscripts

0	refers to vacuum, or an incident property
$1, 2, 3$	refers to surrounding air, thin-film, and substrate, respectively
A	refers to analytically attained value
avg	refers to time-averaged value
c	refers to continuous phase
cr	refers to critical point
d	refers to dispersed phase (nanobubbles)
eff	refers to effective properties
$film$	refers to thin-film
N	refers to numerically attained value
r	refers to relative property, e.g. relative permittivity (dielectric constant)
r	refers to the reflected Poynting vector
t	refers to the transmitted Poynting vector
x	refers to x-direction
y	refers to y-direction
z	refers to z-direction

1 INTRODUCTION

Nanoporous materials consist of nanosize air pockets embedded in a solid matrix. The pores can assume different shapes and sizes and can be closed or open (i.e. connected). Nanoporous media are characterized by their bubble size distribution and porosity which can significantly affect their electrical, thermal, radiation, and optical properties. Progress in synthesizing, characterizing, and modelling such materials would enable technological innovations in various applications ranging from microelectronics to optical devices, and biosensors.

As integrated circuit process technology progresses, the device density increases and chip performance improves continuously [1]. The signal propagation is delayed by the resistance-capacitance time constant RC . The resistance R has been reduced by replacing Al-Cu alloy by Cu metal lines. Further reduction can be achieved via minimizing the capacitance C . This can be accomplished by replacing the current circuit interconnect material, silicon dioxide ($\epsilon_r = 3.9$ at 1 MHz), with new low-k dielectric materials having dielectric constant ϵ_r less than 2.0. Unfortunately, there are no known dense materials that meet the semiconductor manufacturing requirements and have a dielectric constant less than 2. During the last decade, however, nanoporous media made of polymer [2, 3] and SiO_2 [4–9] have been identified as potential solutions. In this approach, nano-size air bubbles ($\epsilon_r = 1.0$) are incorporated

into a continuous matrix, thus reducing the effective dielectric constant of the nanoporous material. Thus, the specific effective dielectric constant is tailored by varying the porosity.

In a similar manner, nanoporous silicon and SiO_2 have been used to manufacture waveguides [9–11], Bragg reflectors [12–18], Fabry-Perot filters [12, 14, 16, 17, 19], and antireflection coatings [20, 21]. For example, in order to confine and propagate electromagnetic (EM) radiation within a waveguide, the guide region itself must have a higher index of refraction than the surrounding cladding [22]. Moreover, Bragg reflectors and Fabry-Perot filters are built by generating alternating layers with prescribed thickness and index of refraction. This geometry takes advantage of constructive and destructive interferences to selectively reflect or transmit at desired wavelengths. Destructive interferences are also used by simple quarter-wave antireflection coatings to reduce or eliminate reflection from a surface. The effect is optimized by utilizing a coating material with index of refraction equal to the geometric mean of the two surrounding indices [22]. In all of these optical applications, the use of nanoporous media enables tuning of the index of refraction by simply controlling the morphology and porosity of the nanosize voids.

In order to design a material with the desired properties one needs to understand and predict the effect of the pores (shape, size, and concentration) on the properties of the host medium. This paper aims at understanding and quantifying these effects. First, the various models commonly used in the lit-

erature are reviewed. Then, numerical simulations of EM wave transport in non-absorbing nanoporous media are presented. Finally, comparisons with effective property models are discussed.

2 CURRENT STATE OF KNOWLEDGE

Effective medium models treat heterogeneous media as homogeneous media with some effective properties. However, there are no explicit criteria as for when this approach is valid. The rule of thumb stating that the overall characteristic length L of the system should be much larger than the average pore diameter D has been used extensively. Typically, one uses the criteria $L \geq 10D$. Unfortunately, this rule seems to be arbitrary and is not supported by any rigorous analysis. Moreover, numerous effective media models have been suggested including (1) the Maxwell-Garnett Theory, (2) the Bruggeman effective medium approximation, (3) the parallel and (4) series models, and (5) those recently derived from the volume averaging method.

The Maxwell-Garnett Theory (MGT) [23] was first developed to model the effective electric permittivity of heterogeneous media consisting of *monodispersed* spheres arranged in a cubic lattice structure within a continuous matrix and of diameter much smaller than the wavelength of the incident EM wave.

Then, the effective dielectric constant $\epsilon_{r,eff}$ is expressed as,

$$\epsilon_{r,eff} = \epsilon_{r,c} \left[1 - \frac{3\phi(\epsilon_{r,c} - \epsilon_{r,d})}{2\epsilon_{r,c} + \epsilon_{r,d} + \phi(\epsilon_{r,c} - \epsilon_{r,d})} \right] \quad (1)$$

where $\epsilon_{r,c}$ and $\epsilon_{r,d}$ are the dielectric constant of the continuous and dispersed phases, respectively, while ϕ is the porosity. The MGT is not valid over the entire range of porosities since the spheres start overlapping for porosity values of $\pi/6 \simeq 52\%$ for 3D cubic lattice arrangement.

To address this issue, Bruggeman [24] considered a similar situation of *polydispersed* spheres distributed in a continuous medium. The effective dielectric constant $\epsilon_{r,eff}$ is obtained by solving the following implicit equation,

$$1 - \phi = \frac{\left(\frac{\epsilon_{r,eff}}{\epsilon_{r,c}} - \frac{\epsilon_{r,d}}{\epsilon_{r,c}} \right)}{\left[\left(\frac{\epsilon_{r,eff}}{\epsilon_{r,c}} \right)^{1/3} \left(1 - \frac{\epsilon_{r,d}}{\epsilon_{r,c}} \right) \right]} \quad (2)$$

Despite applicability to the full range of porosity ($0 \leq \phi \leq 1$) [25], the Bruggeman model is not used as often as MGT in the literature.

Other commonly encountered models are the parallel and series models which have been used, for example, for the effective dielectric constant, index of refraction, as well as thermal and electrical conductivities. The parallel model gives the effective property ψ_{eff} as a linear function of the properties of the continuous and dispersed phases, i.e.,

$$\psi_{eff} = (1 - \phi)\psi_c + \phi\psi_d \quad (3)$$

The series model on the other hand, gives

$$\frac{1}{\psi_{eff}} = \frac{1-\phi}{\psi_c} + \frac{\phi}{\psi_d} \quad (4)$$

Alternatively, del Rio *et al.* [26] suggested the following effective model for electrical conductivity based on the reciprocity theorem,

$$\sigma_{eff} = \sigma_c \frac{1 + \phi \left(\sqrt{\sigma_c/\sigma_d} - 1 \right)}{1 + \phi \left(\sqrt{\sigma_d/\sigma_c} - 1 \right)} \quad (5)$$

The authors successfully validated this model against experimental data for the electrical conductivity of several binary metallic mixtures.

A more rigorous approach, albeit more mathematically involved, was recently derived [27–29] by applying the volume averaging theory (VAT) to the Maxwell’s equations. Models were proposed for the effective dielectric constant $\epsilon_{r,eff}$ and relative permeability $\mu_{r,eff}$ of a two-phase mixture as,

$$\epsilon_{r,eff} = (1 - \phi)\epsilon_{r,c} + \phi\epsilon_{r,d} \quad \text{and} \quad 1/\mu_{r,eff} = (1 - \phi)/\mu_{r,c} + \phi/\mu_{r,d} \quad (6)$$

The range of validity of these expressions was discussed in depth, and a set of inequalities to be satisfied was developed. The authors conclude that “the constraints [posed by these inequalities] are very severe and are not satisfied for many processes. Note also that the Equations (6) do not satisfy the reciprocity theorem [26,30]. This can be attributed to the fact that the reciprocity theorem applies to irrotational vector fields [30]. However, in electromagnetic wave propagation, the curl of the electric and magnetic fields are non-zero as the

time-dependent fields are coupled through Faraday's law of induction and Ampere's law.

Moreover, all the above models disregard the shape, the size distribution, and the spatial distribution of the pores. However, these characteristics were stated to affect the effective properties of the heterogeneous medium [2, 3]. Attempts have been made to account for non-spherical cell geometry by modifying the Maxwell-Garnett [31] and the Bruggeman [32,33] models. For example, Schultz [33] generalized the Bruggeman model for dispersions of randomly oriented spheroids. This model also accounts for the orientation of the cells by incorporating the angle between the revolution axis of the spheroid and the incident energy direction. Similarly, Robles *et al.* [30] proposed a model for randomly distributed and oriented elliptical inclusions using the reciprocity theorem and accounting for possible overlapping. Models such as these are difficult to use in practice because they are involved and/or require specific knowledge of the shape and orientation of the cells.

Finally, note that the above models have been used to predict properties for which they were not necessarily derived. For example, the MGT developed for the electric permittivity ϵ has been used for the index of refraction [34, 35]. Overall, it is not always clear to the user which model is the most appropriate in any particular situation. Experimental data could be used to evaluate the various models, however the conclusions drawn can be contradictory [36]. For example, Si *et al.* [7] concluded that the series model best describes the

dielectric constant of nanoporous silica thin-films with uniformly distributed closed voids. Krause *et al.* [3], on the other hand, concluded that the Maxwell-Garnett model is more appropriate for polymeric closed-cell nanofoam. This apparent contradiction may be attributed to the difficulties and uncertainties in measuring the film porosity, the pore size and shape, and also the optical properties of a nanoporous thin-film. To address this issue, the present study aims at numerically simulating EM wave transport in non-absorbing nanoporous media in order to determine (1) the range of validity of the effective medium approach and (2) the most appropriate effective property model for the dielectric constant and for the index of refraction of non-absorbing nanoporous media.

3 ANALYSIS

3.1 Index of Refraction from the Volume Averaging Theory

A dielectric but non-magnetic material is characterized by its *real* dielectric constant ϵ_r and its *real* index of refraction n such that $n = \sqrt{\epsilon_r}$. Then, recasting the dielectric constants of the continuous and dispersed phases in terms of their indices of refraction, i.e. $\epsilon_{r,c} = n_c^2$ and $\epsilon_{r,d} = n_d^2$, the VAT model for $\epsilon_{r,eff}$ given by Equation (6) can be rewritten for the effective index of refraction as,

$$n_{eff} = \sqrt{\epsilon_{r,eff}} = \sqrt{(1 - \phi)n_c^2 + \phi n_d^2} \quad (7)$$

This relationship can be extended to semi-conductor materials at wavelengths at which they do not absorb.

3.2 Governing Equations and Numerical Implementation

In order to develop the numerical model let us first, consider a surrounding environment (medium 1, n_1) from which the incident EM wave is incident on a non-absorbing dense thin-film (medium 2, n_2) deposited onto a non-absorbing dense substrate (medium 3, n_3). A linearly polarized plane wave in transverse electric mode (TE mode) is incident normal to the film top surface and propagates through the two-dimensional thin-film along the x-direction (see Figure 1). As the wave propagates in the x-y plane, it has only one electric field component in the z-direction, while the magnetic field has two components in the x-y plane (i.e. perpendicularly polarized), such that in a general time-harmonic form,

$$\vec{E}(x, y, t) = E_z(x, y)e^{i\omega t}\vec{e}_z \quad (8)$$

$$\text{and} \quad \vec{H}(x, y, t) = [H_x(x, y)\vec{e}_x + H_y(x, y)\vec{e}_y]e^{i\omega t} \quad (9)$$

Here, \vec{E} is the electric field vector, \vec{H} is the magnetic field vector, and $\omega = 2\pi c_0/\lambda$ is the angular frequency of the wave. The unit vectors for the Cartesian coordinate system are \vec{e}_x , \vec{e}_y and \vec{e}_z . For general time-varying fields in a non-conducting medium, the Maxwell's Equations can be written as

$$\frac{1}{\mu_r\mu_0}\nabla \times [\nabla \times \vec{E}(x, y, t)] - \omega^2\epsilon_r\epsilon_0\vec{E}(x, y, t) = 0 \quad (10)$$

$$\frac{1}{\epsilon_r \epsilon_0} \nabla \times [\nabla \times \vec{H}(x, y, t)] - \omega^2 \mu_r \mu_0 \vec{H}(x, y, t) = 0 \quad (11)$$

where μ_0 and μ_r are the magnetic permeability of vacuum and the relative magnetic permeability, respectively. The associated boundary conditions are

$$\vec{n} \times (\vec{H}_1 - \vec{H}_2) = 0 \quad \text{at the surroundings-film interface} \quad (12)$$

$$\vec{n} \times \vec{H} = 0 \quad \text{at the symmetry boundaries} \quad (13)$$

$$\mu_0^{1/2} (\vec{n} \times \vec{H}) + n_2 \epsilon_0^{1/2} \vec{E} = 0 \quad \text{at the film-substrate interface} \quad (14)$$

$$\mu_0^{1/2} (\vec{n} \times \vec{H}) + n_1 \epsilon_0^{1/2} \vec{E} = 2n_1 \epsilon_0^{1/2} \vec{E}_0 \quad \text{at the source surface} \quad (15)$$

where \vec{n} is the normal vector to the appropriate interface. Equation (14) corresponds to a semi-infinite substrate while Equation (15) models the source surface from which the incident EM wave \vec{E}_0 is emitted, but that will be transparent to the reflected waves.

Moreover, the Poynting vector $\vec{\pi}$ is defined as the cross product of the electric and magnetic field vectors, i.e. $\vec{\pi} = \vec{E} \times \vec{H}$. Its magnitude corresponds to the energy flux carried by the propagating EM wave. Solving Maxwell's equations for the nonzero component of the electric field vector E_z , and relating it to the magnetic field yields,

$$H_y = \frac{n}{\mu_r \mu_0 c_0} E_z \quad (16)$$

Averaging the Poynting vector over an appropriate time interval yields [22],

$$|\pi|_{avg} = \frac{n}{2\mu_r \mu_0 c_0} E_z^2 \quad (17)$$

The incident electric field E_{0z} and therefore the incident time-averaged Poynt-

ing vector $|\pi_0|_{avg}$ are imposed at all locations along the source surface. The values of the Poynting vector along the film-substrate interface are then calculated numerically and averaged along the boundary to yield $|\pi_t|_{avg}$. The transmittance of the thin-film is then recovered by taking the ratio of the transmitted to incident values, $T_{film} = |\pi_t|_{avg}/|\pi_0|_{avg}$. Similarly, the magnitude of the reflected time-averaged Poynting vector $|\pi_r|_{avg}$ is computed numerically, and the reflectance of the film is computed according to $R_{film} = |\pi_r|_{avg}/|\pi_0|_{avg}$. Finally, the above equations were solved numerically using a commercially available finite element solver applying the Galerkin finite element method on unstructured meshes. The two dimensional Maxwell's equations are solved in the frequency domain using a 2D transverse electric (TE) wave formulation as described by Equation (8). In particular, the discretization uses second order elements to solve for the electric field. In order to validate the numerical implementation of the equations and boundary conditions, the interference pattern of a dense and non-absorbing thin-film of SiO₂ with thickness L and index of refraction n_2 deposited on a silicon substrate with index of refraction n_3 and subject to normal incident light of variable wavelength λ was simulated. Numerical results fall within rounding error on the sixth recorded significant digit of the well-known analytical solution expressing the transmissivity and reflectivity as a function of the product n_2L/λ (Ref. [22] p.140).

3.3 Simulations of Nanoporous Thin-films

Figure 1b shows a schematic of a nanoporous thin-film on a semi-infinite substrate. The heterogeneous medium is assumed to be axisymmetric and isotropic with randomly distributed pores which can be modelled as a two-dimensional structure. Moreover, all interfaces were treated as optically smooth. As the EM wave travels through the nanoporous thin film, interferences and scattering take place. However, scattering can be neglected if the size of the individual inhomogeneities dispersed in an otherwise homogeneous matrix is much smaller than the wavelength of the incident radiation [37, 38]. A quantitative criteria requires that the size parameter $\chi = \pi D/\lambda$ be much smaller than unity, where D is the pore diameter (or an equivalent) and λ the incident wavelength [38]. In the present study χ varies between 0.0023 and 0.23, and the fraction of energy scattered by pores of various shape and size was neglected relative to that transmitted and reflected by the film in the incident direction. This assumption was confirmed numerically by comparing the magnitude of the y-component of the Poynting vector perpendicular to the incident directions with its x-component at all locations in the x-y plane. For $\chi=0.23$, the maximum value of the y-component of the Poynting vector was conservatively estimated to be less than 0.5% of the minimum x-component. For the smaller pore sizes this value was several orders of magnitude smaller (0.05% for $\chi=0.023$ and negligibly small for $\chi=0.0023$).

The geometry was further simplified for numerical simulations by building a simple 2D unit cell consisting of domains of dispersed phase embedded in a matrix as shown in Figure 2. Multiple cells were then added on top of each other to simulate nanoporous thin-films of various thicknesses but identical porosities. This results in a regular periodic structure similar to those used in simulations of photonic band gap crystals. However, all cases in the current study are outside of the zero transmission bands for the wavelengths considered [39]. The surrounding environment and the dispersed phase were treated as vacuum ($n_1 = n_d = 1$). Silicon dioxide was used as the thin-film continuous phase characterized by a real index of refraction equal to $n_c = 1.4442$ at $1.55 \mu\text{m}$ [40]. The silicon substrate is weakly absorbing about this wavelength with an absorption index k_3 less than 1.5×10^{-6} [22]. Therefore, as a first order approximation, the silicon substrate was modelled as non-absorbing with an index of refraction $n_3 = 3.48$. Moreover, the wavelength of $1.55 \mu\text{m}$ was chosen because of its predominant use in the telecommunication industry, and ready production by AlGaAs semiconductor laser diodes.

The Maxwell's equations are solved numerically to simulate the EM wave transport in each phase of the nanoporous thin-films. Equation (12) is used as the boundary condition not only at the vacuum-film interface but also at the SiO_2 -pore interfaces. It is important to note that Maxwell's equations are generally applied to macroscopic averages of the fields which can vary widely in the vicinity of individual atoms where they undergo quantum mechanical

effects. These effects are neglected in the present study and all phases are treated as homogeneous and isotropic media for which dielectric constants ϵ_r and indices of refraction n are defined. This is a reasonable assumption for length scales on the order of ten lattice constants, or about 5 nm ([41] p. 387).

Figure 3 is a schematic representation of a model consisting of three unit cells with $\phi = 19.63\%$. It indicates material properties of the various domains and the locations at which each of the boundary conditions are applied. To ensure proper application of the symmetry boundary condition, a 10×10 and a 10×1 unit cell arrangement were modelled. In both cases, the average transmittance and reflectance were identical. Thus, one-unit-cell-wide models are used in all other cases so as to reduce computational time.

Finally, the computed local transmitted Poynting vector is averaged along the film-substrate interface for calculating the film transmittance, T_{film} . The local transmitted energy flux varies slightly as a function of position for the nanoporous geometries considered in this study. For example, the relative difference between the local and averaged transmittance along the nanoporous film/substrate interface for several film thicknesses and constant porosity $\phi=19.63\%$ is less than 1% in the case of spherical pores 100 nm in diameter, 0.01% for 10 nm, and negligibly small for 1 nm.

3.4 Recovery of the Effective Index of Refraction

Numerous methods have been proposed for determining the film thickness and the real and imaginary components of the complex index of refraction from reflectance and transmittance data [42–48]. In the present study, this process is greatly simplified because the absorption coefficient vanishes for both phases and the film thickness is known. Then, the system of equations valid for a non-absorbing homogeneous media on a substrate under *normal incidence* and accounting for interferences is [22],

$$T_{film} = \frac{n_3 t_{12}^2 t_{23}^2}{1 + r_{12}^2 r_{23}^2 + 2r_{12} r_{23} \cos 2\beta} \quad (18)$$

$$R_{film} = \frac{r_{12}^2 + r_{23}^2 + 2r_{12} r_{23} \cos 2\beta}{1 + r_{12}^2 r_{23}^2 + 2r_{12} r_{23} \cos 2\beta} \quad (19)$$

where

$$r_{12} = \frac{1 - n_{eff}}{1 + n_{eff}}, \quad t_{12} = \frac{2}{1 + n_{eff}}, \quad r_{23} = \frac{n_{eff} - n_3}{n_{eff} + n_3}, \quad t_{23} = \frac{2n_{eff}}{n_{eff} + n_3} \quad (20)$$

$$\text{and} \quad \beta = \frac{2\pi n_{eff} L}{\lambda} \quad (21)$$

Here, n_{eff} is the effective index of refraction of the nanoporous film, n_3 is the index of refraction of the silicon substrate, and T_{film} and R_{film} are the transmittance and reflectance, respectively. Equation (20) gives the Fresnel coefficients for non-absorbing media where medium 1 has index of refraction n_1 equal to 1. Finally, β is the phase difference in the wave of incident wavelength λ after one pass through the film of thickness L .

In the present study, the Maxwell's equations are solved numerically and the transmittance T_{film} computed for 201 values of λ in the spectral interval from 1.05 to 2.05 μm . The analytical solution for the transmittance T_{film} is also calculated using Equations (18) through (21) for an arbitrary value of n_{eff} . The quadratic relative differences between the numerical and analytical values of the transmittance are then computed at each wavelength and summed according to

$$F_T = \sum_{i=1}^{201} (T_{film,A,i} - T_{film,N,i})^2 \quad (22)$$

where the subscripts N and A denote numerical and analytical values, respectively. Then, an iterative procedure is followed so as to identify the value of n_{eff} that minimizes the difference F_T . Figure 4 shows the evolution of F_T as a function of the guessed value n_{eff} for a 400 nm thick SiO_2 thin-film with 10 nm pores and 19.63% porosity. It clearly shows that the error reaches a minimum in the interval of possible solutions bounded by the indices of refraction of the dispersed and continuous phase, since *a priori* n_{eff} should fall between n_d and n_c .

4 RESULTS AND DISCUSSION

The numerical simulations performed explore (i) the effect of the film thickness and the validity of the effective medium approach, (ii) the effect of pore shape,

(iii) the effect of the pore spatial distribution, and (iv) the effect of the overall film porosity on the refraction index of non-absorbing nanoporous thin-films.

4.1 Effect of Film Thickness

Figure 5 shows the evolution of the retrieved index of refraction as a function of the ratio of the film thickness L to the diameter of the spherical pores D for a film with 19.63% porosity and three different pore diameters equal to 1, 10, and 100 nm. For each data set, only the film thickness L is varied by varying the number of unit cells stacked in the layer. Then, several conclusions can be drawn:

- (1) For any given pore diameter D and small values of film thickness L , the effective index of refraction is a function of L and D . Therefore the effective medium approach is not valid.
- (2) Beyond a critical thickness L_{cr} , the effective medium approach is valid and an effective index of refraction can be defined as a function of porosity ϕ and of the constituent phase indices of refraction n_c and n_d only.
- (3) The magnitude of the critical film thickness L_{cr} is a function of the pore diameter and the incident radiation wavelength λ . In Figure 5, the L_{cr}/D values are arbitrarily defined so that all subsequent values of n_{eff} fall within 0.05% of the converged solution. In the present case, L_{cr} is found to be up to 50 times the pore diameter for 100 nm pores.

4.2 Effect of Pore Shape

Several experimental studies of nanoporous media have concluded that flattened cells affect the effective dielectric constant and index of refraction of the medium [2, 3]. To explore this question, simulations were performed for various pore shapes including elliptical pores, overlapping spherical pores, and columnar pores. Also, this resulted in simulations of both open and closed-cell nanoporous structures.

First, elliptical pores characterized by thickness b and width a , as depicted in Figure 2b, are considered. The porosity was varied by changing the length and width of the unit cell. The degree of scattering was found to be negligible in most cases by comparing the magnitude of the x and y-components of the Poynting vector at all locations in the computational domain. When it was not deemed negligible, the uncertainty due to scattering was calculated and considered when determining the critical thickness L_{cr} . First, two values (1 and 10 nm) of the parameter b were considered while maintaining a constant ratio $a/b = 2$ and porosity $\phi = 19.63\%$. As in the case of spherical pores, variations in the effective properties are observed for low values of L/b , and a single value is reached for larger values of L/b , as shown in Figure 6. Additionally, cases were computed this time with $b = 10$ nm, and $a/b = 1/6, 2, 6,$ and 12 at various porosities (not shown). In all cases, the converged effective properties were equal to those found using spherical pores ($a/b = 1$) with the same

porosity.

Moreover, in order to simulate porous silicon, which features open-cell morphology, simulations were performed for geometries consisting of columnar pores, as shown in Figure 2c. The same value of the index of refraction was retrieved for all film thicknesses, i.e., the effective medium approximation is valid for all film thicknesses. In addition, the retrieved value of n_{eff} was identical to that for nanoporous thin-film of equal porosity but containing spherical or elliptical pores.

An open-cell morphology intended to represent overlapping spherical pores, such as those found in aerogels, was also simulated (see Figure 2d). The same effective index of refraction was retrieved for all thicknesses; its value was equal to that found for all other pore shapes and nanoporous thin-films of identical porosity.

Another simulated pore geometry included spherical pores with partially overlapping cross sections as illustrated in Figure 2e. Once again, it was found that the effective index of refraction converged to the same value as that of the previously considered morphologies with identical porosity.

Finally, fluctuations in the value of n_{eff} for small values of L/D are caused by interferences due to reflections off the interfaces perpendicularly oriented to the direction of wave propagation. Beyond L_{cr} this effect averages out, and a constant value of n_{eff} is displayed. This is first demonstrated by the lack

of variation seen in n_{eff} for the simulations of open-cell geometries depicted in Figure 2c and 2d. These geometries have no internal surfaces from which waves can reflect, thus inhibiting the interference effect. As a result, the retrieved n_{eff} is constant for all film thicknesses. For closed pores, however, the fluctuation in the retrieved index of refraction as a function of film thickness increases significantly as the pore diameter increases. This phenomenon can be explained simply by considering the length scales of the films relative to the wavelength of the incident radiation. For example, for spherical pores with $D = 1, 10,$ and 100 nm, L_{cr} can be found to be approximately 10 nm, 600 nm, and $30 \mu\text{m}$, respectively for an incident radiation wavelength of $1.55 \mu\text{m}$ (Figure 5). In the case of 1 nm pore size, the phase difference β between interfering waves is negligibly small. In the case of the 100 nm pore size, however, the phase difference is larger and responsible for the large fluctuations in n_{eff} versus L/D as illustrated in Figure 5. Thus, the critical thickness L_{cr} , beyond which the effective medium approach is valid, depends also on the wavelength λ .

4.3 *Effect of Pore Spatial Arrangement*

Thus far, all simulations were performed on models built from basic unit cells. To explore a situation where the pores are not arranged in a regular cubic distribution, several simulations were performed on films of varying thickness with pores distributed at random locations between 0 and L along the x-axis.

Values that would have resulted in overlapping pores were eliminated so as to maintain a closed-cell structure. Cases with pores' diameters of 1 and 10 nm were simulated. Figure 7 compares the evolution of the effective index of refraction as a function of L/D for randomly located pores and that for regular cubic pore distribution while maintaining constant porosity ($\phi=19.63\%$). Larger values of L_{cr} are obtained for each pore diameter in the cases of randomly distributed pores. However, beyond L_{cr} the retrieved effective index of refraction is the same as that found using previously discussed pore morphologies of equal porosity. The 1 nm pore case is fully converged to this value at $L_{cr}/D=100$, and the 10 nm case is within 0.5% at $L/D=200$.

4.4 *Effect of Porosity*

From the above analysis, one can conclude that beyond a critical thickness, the effective medium approach is valid and the effective index of refraction depends only on the porosity and index of refraction of each of the two constituent phases, but not on the pore shape, size distribution, or spatial distribution. This confirms the general form of commonly used effective medium models such that $n_{eff} = f(\phi, n_c, n_d)$ [see Eqs. (1) to (6)].

To assess the validity of the commonly used models, simulations were run for silicon dioxide with 10 nm spherical closed pores, and for porous silicon with columnar pores. For silicon, the incident wavelength was chosen to be $\lambda = 2.71$

μm at which the complex index of refraction is $m_{Si} = 3.44 - i2.5 \times 10^{-9}$ [22].

Thus, the absorption coefficient can also safely be neglected. Figure 8 shows the converged values of the effective index of refraction plotted versus porosity along with predictions of the above discussed models. The Bruggeman model differed from the MGT model by a maximum of only 2.3% for silicon, and by only 0.1% for SiO_2 . Thus, the Bruggeman model will not be discussed further.

The numerical values retrieved for n_{eff} match those predicted by the volume averaging technique [Equation (7)] within rounding error. The relative difference between the parallel, Maxwell-Garnett, reciprocity, and series models and the numerical results for nanoporous SiO_2 was up to 1.7%, 2.6%, 3.3%, and 4.9%, respectively. In the case of porous silicon, these differences are larger and can reach up to 16.4%, 22.4%, 29.3%, and 39.5%, respectively. Therefore, as the index of refraction of the continuous phase material increases, the percent difference between the various effective medium models and the numerically predicted value of n_{eff} increases.

Moreover, simulations were also conducted to investigate a hypothetical medium in which the dispersed phase has a larger index of refraction than the continuous phase. Specifically, the supposed case of spherical silicon particles ($n_d=3.44$) distributed in an otherwise continuous SiO_2 matrix ($n_c=1.426$) was considered. The incident wavelength was chosen as $2.71 \mu\text{m}$ such that both phases could be considered as non-absorbing. As in the previous cases, the effective index of refraction initially varied for relatively thin films before con-

verging to a value equal to that predicted by the VAT model. Note that here, the effective index of refraction increases with porosity since $n_d > n_c$.

Finally, the conditions for the validity of the VAT model proposed by del Rio and Whitaker [27, 28] based on order of magnitude estimates seem to be too stringent [36]. Indeed, even though they are not satisfied, the formulae for the effective properties compare very well with those computed from numerical results.

5 CONCLUSIONS

Numerous effective medium models have been proposed and used in the literature. However, it remained unclear which model is applicable to a specific situation. In order to address this issue, numerical solutions of the Maxwell's equations for axisymmetric nanoporous thin-films of various porosity and with open and closed pores of various shape, size, and spatial distribution have been presented and discussed. Several conclusions can be drawn.

First, there exists a critical nanoporous film thickness L_{cr} below which the effective index of refraction is a function of (i) the film thickness, (ii) the pore shape, (iii) their size, (iv) their spatial distribution, and (v) the wavelength considered. For film thickness less than L_{cr} , the effective medium approach is not applicable and the heterogeneous nature of the medium should be taken into account.

For films thicker than the critical thickness L_{cr} , the effective medium approach is valid and an effective index of refraction can be defined only as a function of porosity ϕ and of the indices of refraction of the constituent phases, n_c and n_d . In other words, *the pore shape, size, and spatial distribution have no effect on the effective index of refraction of the nanoporous medium.*

Unfortunately, it was not possible to find a simple correlation between the critical thickness L_{cr} and the pore shape, size, spatial distribution, or the wavelength considered. Qualitatively, L_{cr} increases as the pore size increases for pores that are randomly distributed.

Finally, the models obtained from the VAT are recommended for calculating the effective index of refraction and the effective dielectric constant of the two-phase non-absorbing nanoporous media when the effective medium approximation is valid ($L > L_{cr}$). Then,

$$n_{eff} = \sqrt{(1 - \phi)n_c^2 + \phi n_d^2} \quad \text{and} \quad \epsilon_{r,eff} = (1 - \phi)\epsilon_{r,c} + \phi\epsilon_{r,d} \quad (23)$$

Practically, models other than the VAT model give acceptable predictions when the continuous and dispersed phases have similar indices of refraction. However, the predictions can be significantly erroneous for nanoporous media when one of the constituting phases features an index of refraction significantly different from the other.

The discrepancies between the different models and reported experimental

data for $\epsilon_{r,eff}$ and n_{eff} can be attributed to (1) the fact that the film thickness was smaller than L_{cr} such that the effective medium approach is not valid, and (2) experimental uncertainty associated with the porosity ϕ , and with the properties of the continuous phase. Uncertainty in these values could result in significant error in the model predictions. Together, these effects could lead to erroneous and often contradictory conclusions about the effect of the size and shape of the pores on the effective optical properties of nanoporous media.

Acknowledgements

The authors would like to thank the Femlab support team for their valuable support in performing the numerical simulations. Thanks are also extended to Dr. Stéphane Durant for useful discussion and exchange of information. This work was supported in part by the National Science Foundation. L. Pilon acknowledges the support of NSF through the CAREER Award.

References

- [1] B. Y. Tsui, C. C. Yang, K. L. Fang, Anisotropic thermal conductivity of nanoporous silica film, *IEEE Transactions on Electron Devices* 51 (1) (2004) 20.
- [2] H. J. Cha, J. Hedrick, R. A. DiPietro, T. Blume, R. Beyers, D. Y. Yoon, Structures and dielectric properties of thin polyimide films with nanofoam

morphology, Appl. Phys. Lett. 68 (14) (1996) 1930.

- [3] B. Krause, G. H. Koops, N. F. A. van der Vegt, M. Wessling, M. Wubbenhorst, J. van Turnhout, Ultralow-k dielectrics made by supercritical foaming of thin polymer films, Adv. Mater. 14 (15) (2002) 1041.
- [4] H. Fan, H. R. Bently, K. R. Kathan, P. Clem, Y. Lu, C. J. Brinker, Self-assembled aerogel-like low dielectric constant films, J. Non-Cryst. Solids 285 (2001) 79.
- [5] C. Flannery, C. Murray, I. Streiter, W. E. Schulz, Characterization of thin-film aerogel porosity and stiffness with laser-generated surface acoustic waves, Thin Solid Films 388 (2001) 1.
- [6] L. W. Hrubesh, L. E. Keene, V. R. Latorre, Dielectric properties of aerogels, J. Mater. Res. 8 (7) (1993) 1736.
- [7] J. J. Si, H. Ono, K. Uchida, S. Nozaki, H. Morisaki, N. Itoh, Correlation between the dielectric constant and porosity of nanoporous silica thin films deposited by the gas evaporation technique, Appl. Phys. Lett. 79 (19) (2001) 3140.
- [8] D. M. Smith, J. Anderson, C. C. Cho, G. P. Johnston, S. P. Jeng, Preparation of low-density xerogels at ambient pressure for low-k dielectrics, Applications Mater. Res. Soc. Symp. Proc. 381 (1995) 261.
- [9] A. Jain, S. Rogojevic, S. Ponoth, I. Matthew, W. N. Gill, P. Persans, M. Tomozawa, J. L. Plawsky, E. Simonyi, Porous silica materials as low- k dielectrics for electronic and optical interconnects, Thin Solid Films 398 (2001) 513.

- [10] A. Loni, L. Canham, M. Berger, R. Arens-Fischer, H. Munder, H. Luth, H. Arrand, T. Benson, Porous silicon multilayer optical waveguides, *Thin Solid Films* 276 (1996) 143.
- [11] H. F. Arrand, T. M. Benson, A. Loni, M. G. Krueger, M. Thoenissen, H. Lueth, Self-aligned porous silicon optical waveguides, *Electron. Lett.* 33 (20) (1997) 1724.
- [12] M. G. Berger, M. Thonissen, R. Arens-Fischer, H. Munder, H. Luth, M. Arntzen, W. Thei, Investigation and design of optical properties of porosity superlattices, *Thin Solid Films* 255 (1995) 313.
- [13] J. Diener, N. Künzner, D. Kovalev, E. Gross, V. Y. Timoshenko, G. Polisski, F. Koch, Dichroic Bragg reflectors based on birefringent porous silicon, *Applied Phys. Lett.* 78 (24) (2001) 3887.
- [14] M. Krüger, M. Marso, M. G. Berger, M. Thönissen, S. Billat, R. Loo, W. Reetz, H. Lüth, S. Hilbrich, R. Arens-Fischer, P. Grosse, Color-sensitive photodetector based on porous silicon superlattices, *Thin Solid Films* 297 (1997) 241.
- [15] S. Zangoie, M. Schubert, C. Trimble, D. Thompson, J. Woollam, Infrared ellipsometry characterization of porous silicon Bragg reflectors, *Appl. Opt.* 40 (6) (2001) 906.
- [16] S. Zangoie, R. Jansson, H. Arwin, Ellipsometric characterization of anisotropic porous silicon Fabry-Perot filters and investigation of temperature effects on capillary condensation efficiency, *J. Appl. Phys.* 86 (2) (1999) 850.
- [17] C. Mazzoleni, L. Pavesi, Application to optical components of dielectric porous

silicon multilayers, *Appl. Phys. Lett.* 67 (20) (1995) 2983.

- [18] K. Kordás, S. Beke, A. Pap, A. Uusimäki, S. Leppävuori, Optical properties of porous silicon. Part II: Fabrication and investigation of multilayer structures, *Opt. Mater.* 25 (2004) 257.
- [19] A. Janshoff, K. P. S. Dancil, C. Steinem, E. P. Greiner, V. S. Y. Lin, C. Gurtner, K. Motesharei, M. J. Sailor, M. R. Ghadiri, Macroporous p-type silicon Fabry-Perot layers. fabrication, characterization, and applications in biosensing, *J. Amer. Chem. Soc.* 120 (1998) 12108.
- [20] I. M. Thomas, Method for the preparation of porous silica antireflection coatings varying in refractive index from 1.22 to 1.44, *Appl. Opt.* 31 (28) (1992) 6145.
- [21] Q. Zhang, J. Wang, G. Wu, J. Shen, S. Buddhudu, Interference coating by hydrophobic aerogel-like SiO₂ thin films, *Mater. Chem. Phys.* 72 (2001) 56.
- [22] M. Q. Brewster, *Thermal Radiative Transfer and Properties*, John Wiley and Sons, Inc., 1992.
- [23] J. C. M. Garnett, Colours in metal glasses and in metallic films, *Philos. Trans. R. Soc. London, Ser. A* 203 (1904) 385.
- [24] D. A. G. Bruggeman, Berechnung verschiedener physikalischer konstan ten von heterogenen substanzen, *Ann. Phys. (Leipzig)* 24 (1935) 636.
- [25] F. Cernuschi, S. Ahmaniemi, P. Vuoristo, T. Mantyla, Modelling of thermal conductivity of porous materials: application to thick thermal barrier coatings, *J. Eur. Ceram. Soc.* 24 (2004) 2657.

- [26] J. A. del Rio, R. W. Zimmerman, R. A. Dawe, Formula for the conductivity of a two-component material based on the reciprocity theorem, *Solid State Comm.* 106 (4) (1998) 183.
- [27] J. A. del Rio, S. Whitaker, Maxwell's equations in two-phase systems I: Local electrodynamic equilibrium, *Trans. Por. Med.* 39 (2000) 159.
- [28] J. A. del Rio, S. Whitaker, Maxwell's equations in two-phase systems II: Two-equation model, *Trans. Por. Med.* 39 (2000) 259.
- [29] V. S. Travkin, I. Catton, Transport phenomena in heterogeneous media based on volume averaging theory, *Adv. Heat Trans.* 34 (2001) 1.
- [30] M. Robles, J. Taguena-Martinez, J. A. del Rio, Effective conductivity of chemically deposited ZnO thin films, *Thin Solid Films* 293 (1997) 320.
- [31] G. Grimvall, *Thermophysical Properties of Materials. Selected Topics in Solid State Physics*, Vol. XVIII, North-Holland Physics Publishing, 1986.
- [32] R. E. Meredith, *Studies in the conductivities of dispersions*, Lawrence Radiation Laboratory Report, UCRL-8667, 1959.
- [33] B. Schulz, Thermal conductivity of porous and highly porous materials, *High Temp. High Press.* 13 (1981) 649.
- [34] S. Labbe-Lavigne, S. Barret, F. Garet, L. Duvillaret, J. Coutaz, Far-infrared dielectric constant of porous silicon layers measured by terahertz time-domain spectroscopy, *J. Appl. Phys.* 83 (1998) 6007.
- [35] C. Hincinschi, M. Friedrich, C. Murray, I. Streiter, S. E. Schulz, T. Gessner, D. R. T. Zahn, Characterization of silica xerogel films by variable-angle

spectroscopic ellipsometry and infrared spectroscopy, *Semicond. Sci. Technol.* 16 (11) (2001) 806.

[36] M. Braun, Effective optical properties of nanoporous thin-films, Master's thesis, Department of Mechanical and Aerospace Engineering, University of California, Los Angeles, CA (2004).

[37] R. Viskanta, M. P. Mengüç, Radiative transfer in dispersed media, *Appl. Mech. Rev.* 42 (9) (1989) 241.

[38] M. F. Modest, *Radiative Heat Transfer*, McGraw-Hill, New York, NY, 2002.

[39] S. G. Johnson, J. D. Joannopoulos, *Photonic Crystals: The Road from Theory to Practice*, Kluwer Academic Publishers, 2002.

[40] J. H. Wray, J. T. Neu, Refractive index of several glasses as a function of wavelength and temperature, *J. Opt. Soc. Amer.* 59 (6) (1969) 774.

[41] C. Kittel, *Introduction to Solid State Physics*, John Wiley and Sons, 1996.

[42] M. A. Khashan, A. M. El-Naggar, E. Shaddad, A new method of determining the optical constants of a thin film from its reflectance and transmittance interferograms in a wide spectral range: 0.2-3 μm , *Opt. Commun.* 178 (2000) 123.

[43] M. A. Khashan, A. M. El-Naggar, A new method of finding the optical constants of a solid from the reflectance and transmittance spectrograms of its slab, *Opt. Commun.* 174 (2000) 445.

[44] A. B. Djurisić, T. Fritz, K. Leo, Determination of optical constants of

thin absorbing films from normal incidence reflectance and transmittance measurements, *Opt. Commun.* 166 (1999) 35.

[45] J. C. Manificier, J. Gasiot, J. P. Fillard, A simple method for the determination of the optical constants n , k and the thickness of a weakly absorbing thin film, *J. Phys. E: Sci. Instrum.* 9 (1976) 1002.

[46] R. Swanepoel, Determination of the thickness and optical constants of amorphous silicon, *J. Phys. E: Sci. Instrum.* 16 (1983) 1214.

[47] J. J. Ruíz-Pérez, J. M. González-Leal, D. A. Minkov, E. Márquez, Method for determining the optical constants of thin dielectric films with variable thickness using only their shrunk reflection spectra, *J. Phys. D: Appl. Phys.* 34 (2001) 2489.

[48] B. S. Richards, A. Lambertz, A. B. Sproul, Determination of the optical properties of non-uniformly thick non-hydrogenated sputtered silicon thin films on glass, *Thin Solid Films* 460 (2004) 247.

Figure and Table Captions

Figure 1. Schematic of two-dimensional (a) dense and (b) closed-cell nanoporous thin-film exposed to a linearly polarized plane wave.

Figure 2. Geometry of the various unit cells investigated.

Figure 3. Schematic of model composed of three unit cells. Each contains a centered pore and has porosity 19.63%. The schematic also depicts where boundary conditions and domain properties are assigned.

Figure 4. Error as calculated according to Eq.(22) versus effective index of refraction n_{eff} .

Figure 5. Evolution of effective index of refraction as a function of L/D for films with 19.63% porosity and three different pore diameters.

Figure 6. Evolution of effective index of refraction as a function of L/b for elliptical pores with aspect ratio $a/b = 2$ and $b = 1$ and 10 nm for an overall porosity of $\phi = 19.63\%$.

Figure 7. Evolution of effective index of refraction as a function of L/D for regular and random pore distribution and porosity $\phi = 19.63\%$.

Figure 8. Numerical result for effective index of refraction as a function of porosity for (a) nanoporous SiO_2 at $\lambda = 1.55 \mu\text{m}$ and (b) nanoporous Si at $\lambda = 2.71 \mu\text{m}$.

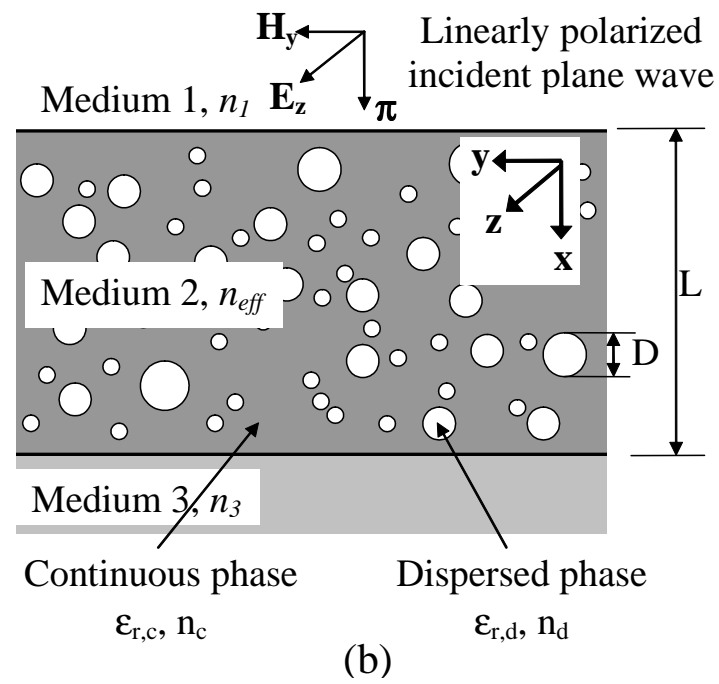
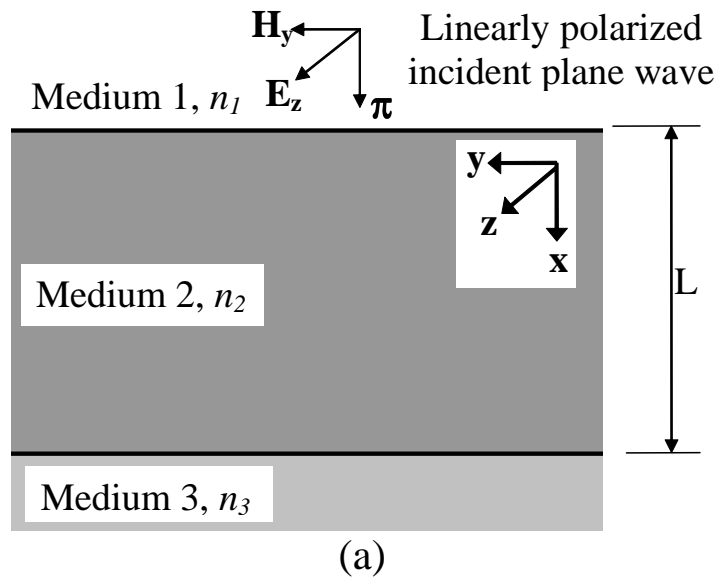


Fig. 1. Schematic of two-dimensional (a) dense and (b) closed-cell nanoporous thin-film exposed to a linearly polarized plane wave.

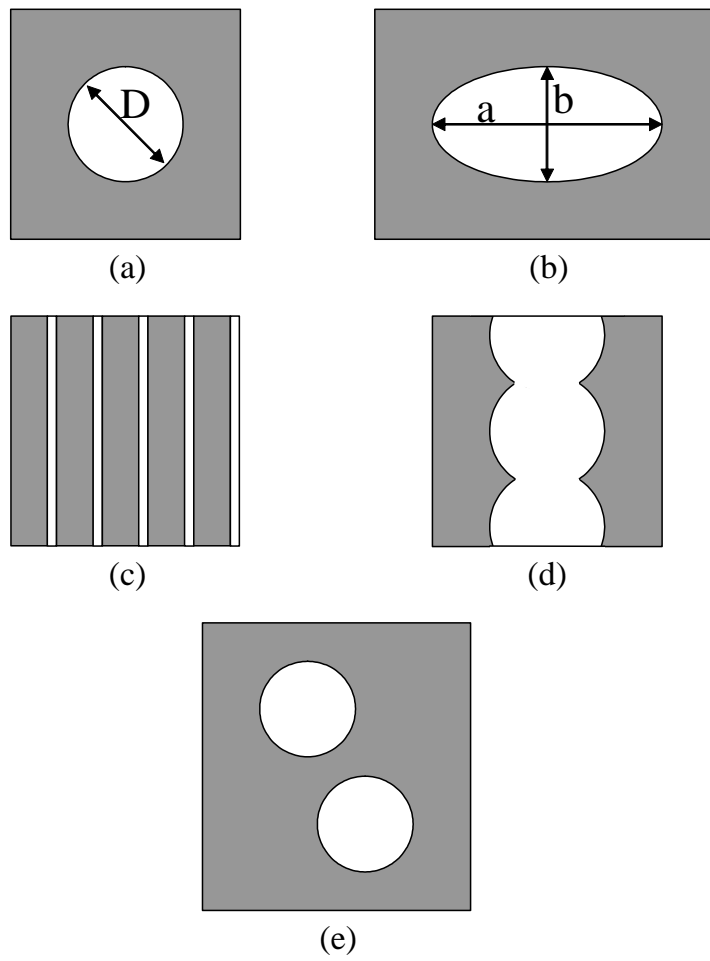


Fig. 2. Geometry of the various unit cells investigated.

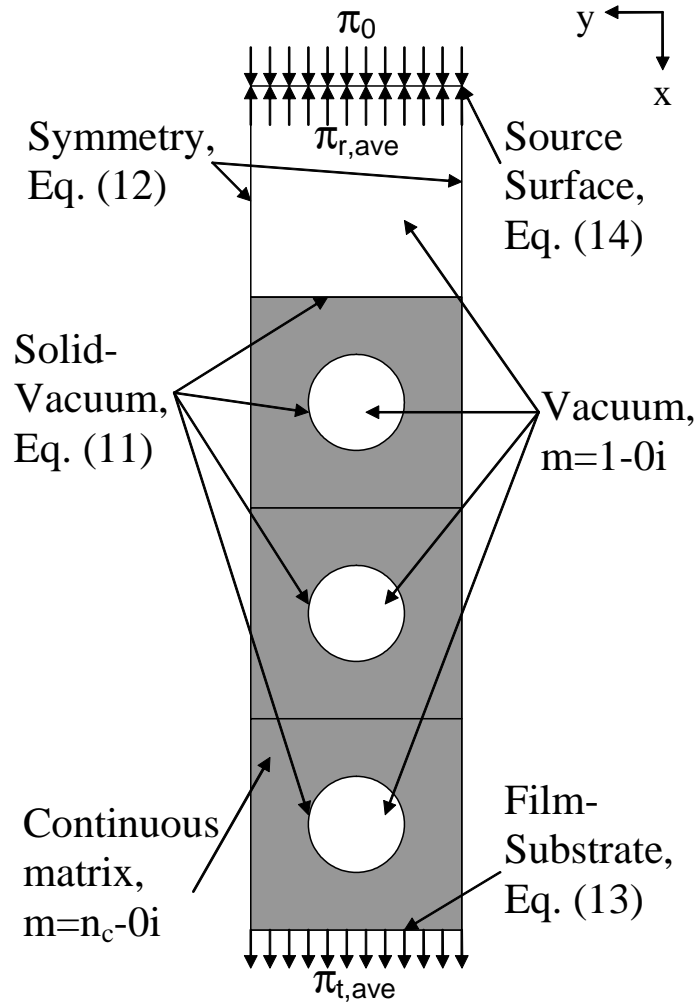


Fig. 3. Schematic of model composed of three unit cells. Each contains a centered pore and has porosity 19.63%. The schematic also depicts where boundary conditions and domain properties are assigned.

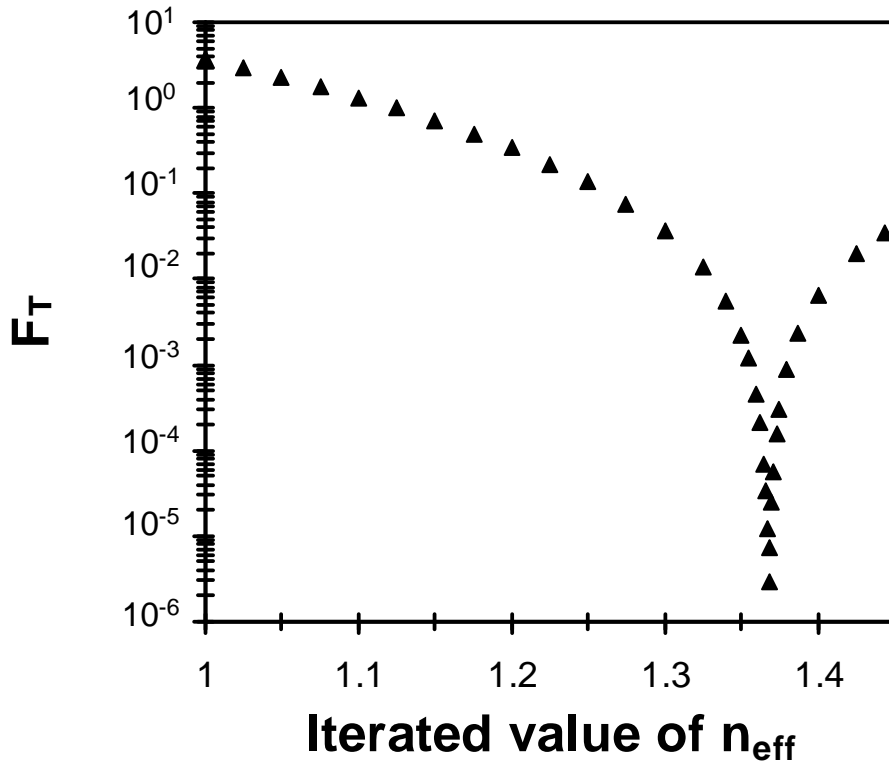


Fig. 4. Error as calculated according to Eq. (22) versus effective index of refraction

n_{eff} .

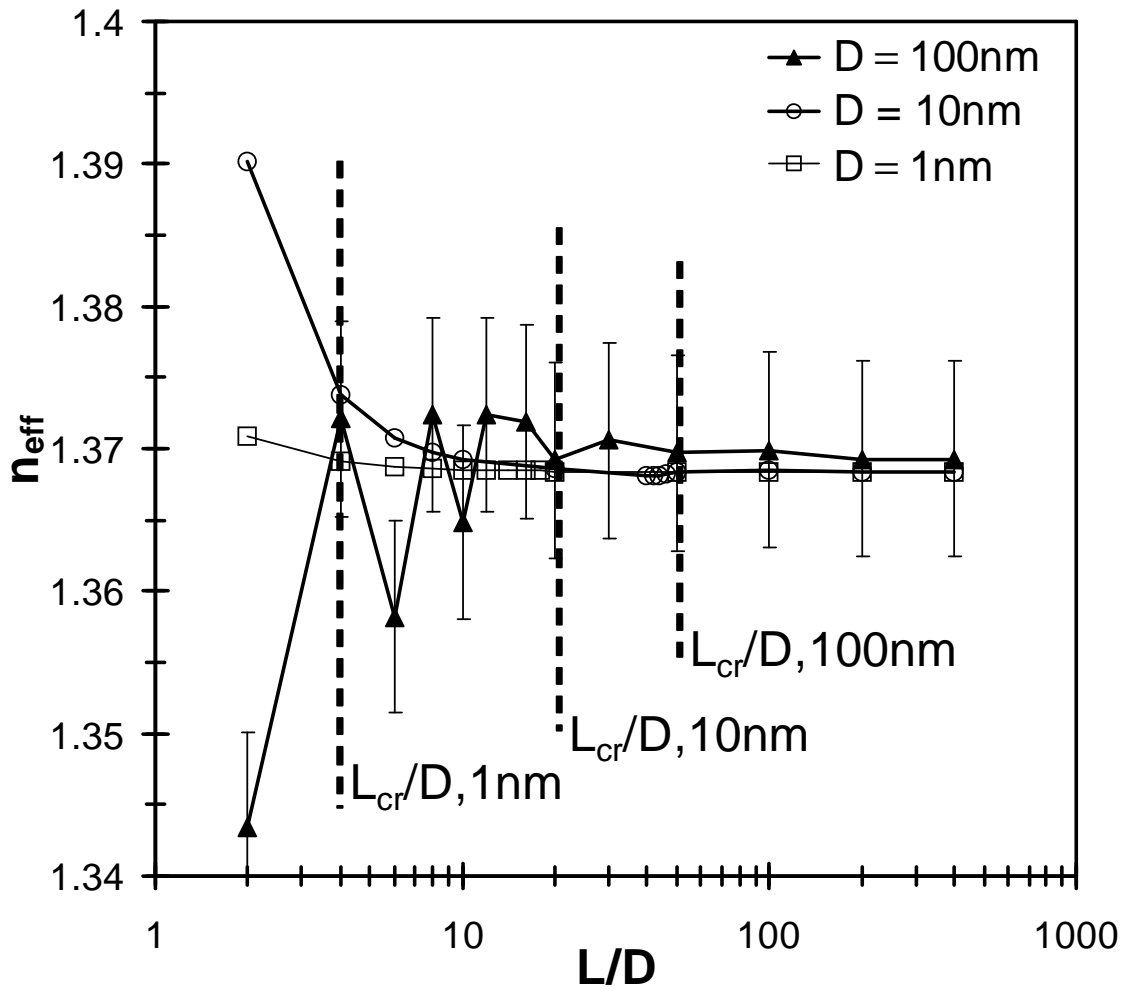


Fig. 5. Evolution of effective index of refraction as a function of L/D for films with 19.63% porosity and three different pore diameters.

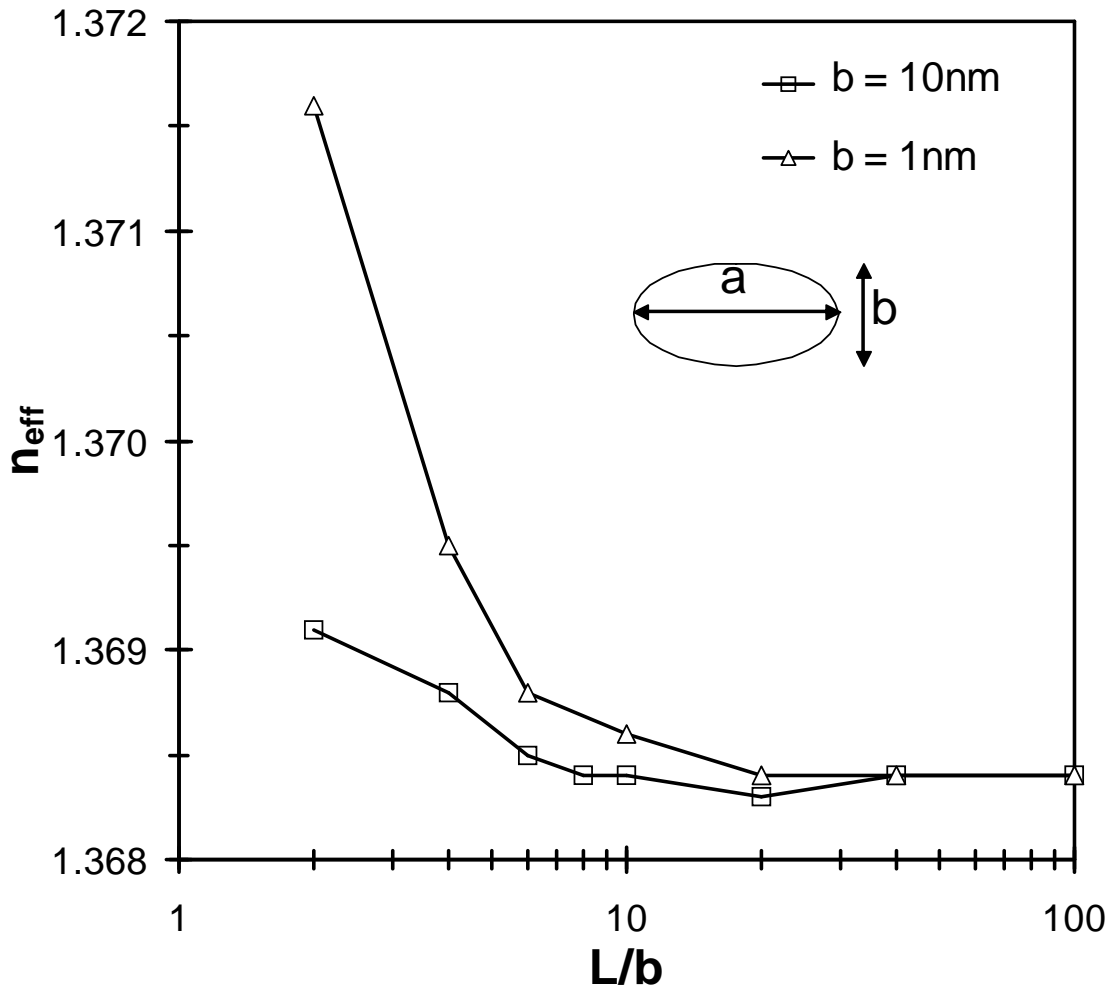


Fig. 6. Evolution of effective index of refraction as a function of L/b for for elliptical pores with aspect ratio $a/b = 2$ and $b = 1$ and 10 nm for an overall porosity of $\phi = 19.63\%$.

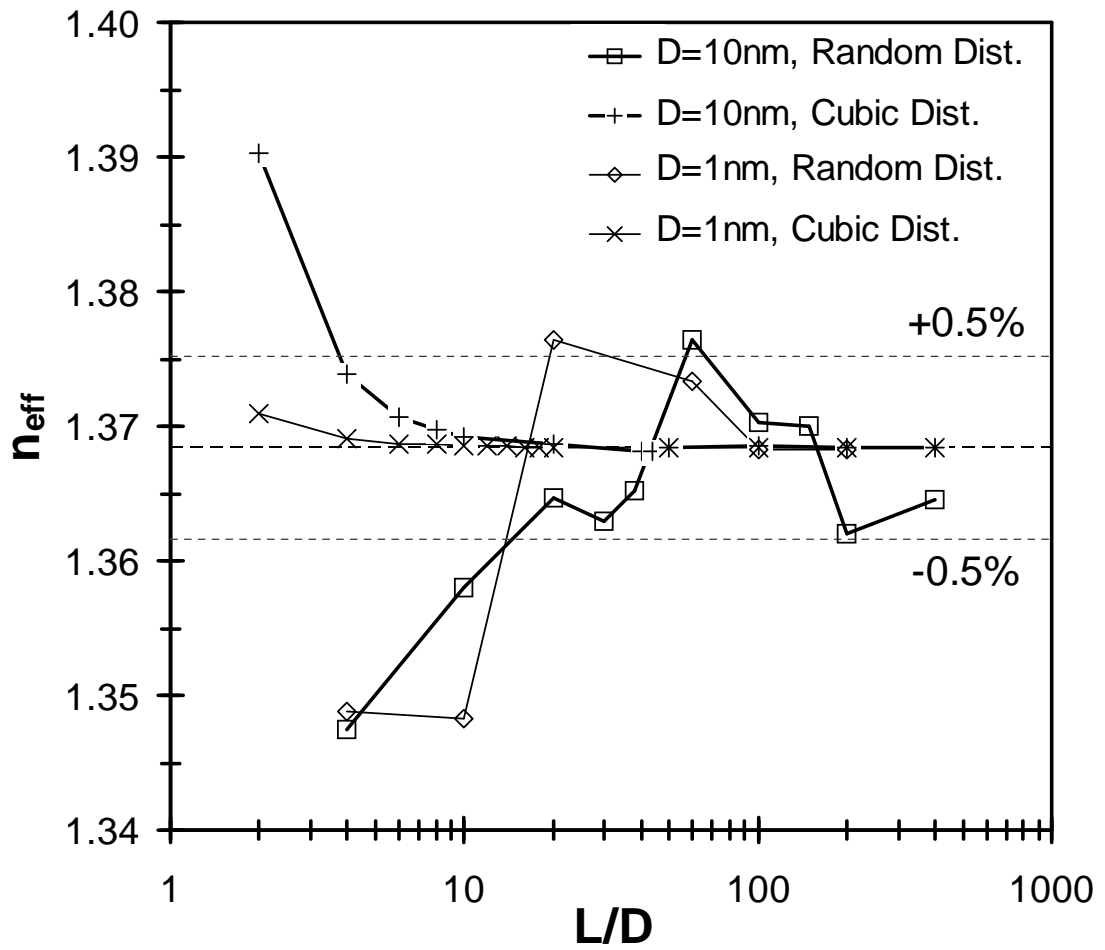


Fig. 7. Evolution of effective index of refraction as a function of L/D for regular and random pore distribution and porosity $\phi = 19.63\%$.

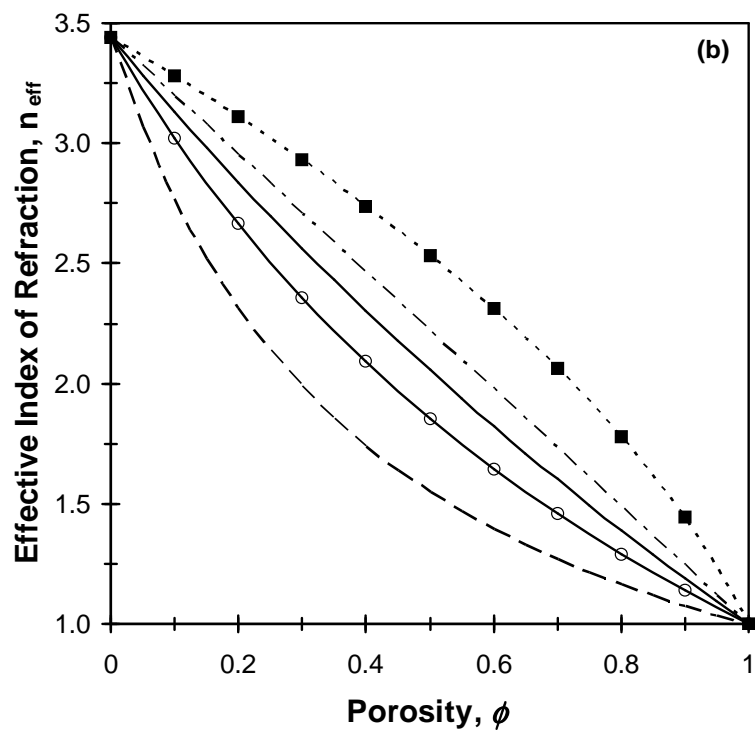
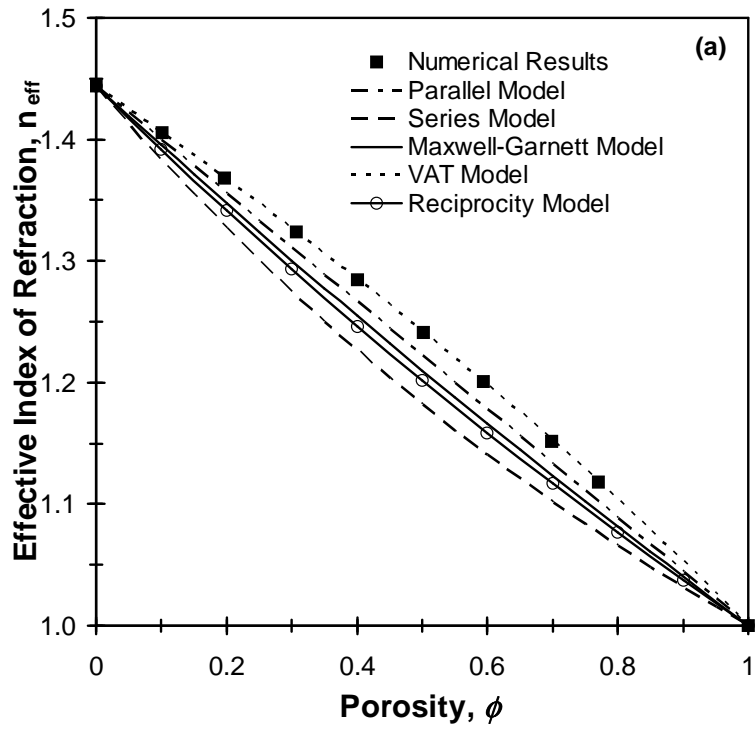


Fig. 8. Numerical result for effective index of refraction as a function of porosity for (a) nanoporous SiO_2 at $\lambda = 1.55 \mu\text{m}$ and (b) nanoporous Si at $\lambda = 2.71 \mu\text{m}$.